frontiers | Frontiers in Materials

TYPE Original Research
PUBLISHED 19 January 2023
DOI 10.3389/fmats.2023.1103590

OPEN ACCESS

EDITED BY
Jianxin Yi,
University of Science and Technology of China, China

REVIEWED BY
Sufang He,
Kunming University of Science and Technology, China
Gang Feng,
Nanchang University, China

*CORRESPONDENCE
Xiaowei Cheng,
chengxw@swpu.edu.cn

SPECIALTY SECTION
This article was submitted to Ceramics and Glass, a section of the journal Frontiers in Materials

RECEIVED 21 November 2022
ACCEPTED 09 January 2023
PUBLISHED 19 January 2023

CITATION
Wu Z, Jiang L, Dong Q, Gao Q, Cai J and Cheng X (2023), Effect and mechanism of rare Earth and alkaline Earth metals on the high-temperature stability of activated alumina.
Front. Mater. 10:1103590.
doi: 10.3389/fmats.2023.1103590

Effect and mechanism of rare Earth and alkaline Earth metals on the high-temperature stability of activated alumina

Zhiqiang Wu[1], Longwen Jiang[1], Quan Dong[2], Qiang Gao[3], Jingxuan Cai[3] and Xiaowei Cheng[3]*

[1]CNOOC Research Institute Co., Ltd., Beijing, China, [2]Exploration Business Department of PetroChina Southwest Oil and Gas Field Company, Chengdu, China, [3]School of New Energy and Materials, Southwest Petroleum University, Chengdu, China

Active alumina (Al_2O_3) is one of the carrier materials used for the purification of automobile exhaust. The crystal transformation of active Al_2O_3 is due to the high temperature of the automobile exhaust port, which greatly reduces the specific surface area and affects the catalytic efficiency. To improve the high-temperature stability of active Al_2O_3, this study synthesized Al_2O_3 *via* the gel-sol method. The influence of rare Earth and alkaline Earth metal doping modification on the high-temperature stability of activated Al_2O_3 was investigated. The specific surface areas were analyzed using Brunauer–Emmett–Teller, X-ray diffraction, Fourier-transform infrared spectroscopy, Scanning electron microscopy, and transmission electron microscopy to explore the effects and mechanism of different contents of La, Ce, and Ba on active Al_2O_3. The results showed that suitable single doping of La, Ce, and Ba inhibited the phase transition of Al_2O_3 and improved the high-temperature stability of active Al_2O_3. When 1% of La and Ba were mixed and doped into active Al_2O_3, the specific surface area of the sample after aging at 1,100°C for 4 h was 119.2512 m^2/g. X-ray diffraction analysis revealed the agglomeration of Ba atoms inside the alumina and that the incorporated La atoms accelerated the agglomeration and promoted the formation of $BaAl_2O_4$.

KEYWORDS

activated alumina, sol-gel, rare Earth metals, alkaline Earth metals, doping modification

1 Introduction

China is the world's largest producer and consumer of motor vehicles (Ministry of Environmental Protection of the People's Republic of China, 2020). In 2019, the total emission of four pollutants from motor vehicles in China was initially calculated to be 16.038 million tons. These four pollutants are the main source of air pollution in the large and medium-sized cities of China. Engine external purification technology is one of the effective strategies for treating automobile exhaust, which minimizes the emission of pollutants (Tu and Ming, 2013; Deng and Zhou, 2020). The off-machine purification technology converts the harmful substances in automobile exhaust into other harmless or less harmful substances through catalysis (Wang et al., 2017). The efficiency of the catalysis can be improved by dispersing a catalyst on the surface of activated alumina (Azizi et al., 2016; Feng et al., 2019; Yadav et al., 2021). The large specific surface area of activated alumina provides sufficient attachment sites for the catalyst to maintain good dispersion, thereby improving catalytic efficiency (Lin et al., 2021). However, the exhaust port temperature of automobile engine is

TABLE 1 Experimental formula for the sol-gel synthesis of γ-Al_2O_3.

Name	Aluminum nitrate	Ethanol	Deionized water	Propylene oxide	Ammonia
Dosage/mol	1	40	60	17	13

TABLE 2 Experimental formula of different amounts of lanthanum nitrate.

Number	Dosage (mole percentage of aluminum nitrate)
La-1%	1
La-2%	2
La-4%	4
La-8%	8
La-16%	16

TABLE 3 Experimental formula of different addition amounts of cerium nitrate.

Number	Dosage (mole percentage of aluminum nitrate)
Ce-1%	1
Ce-2%	2
Ce-4%	4
Ce-8%	8
Ce-16%	16

usually up to 800°C–1,000°C. When the temperature exceeds 1,000°C, the crystal transformation of active Al2O3 will occur, resulting in a substantial reduction of specific surface area, which seriously affects the catalytic efficiency (Xu et al., 2022). Therefore, the improvement of the high-temperature stability of the active Al_2O_3 is urgent and crucial.

Studies have shown that the activated alumina synthesized *via* the sol-gel method has a controllable grain size, uniform internal pores, and better performance. The synthesis method is simple and safe (Hosseini et al., 2011; Aghamohammadi et al., 2017). However, the pure activated alumina prepared *via* the sol-gel method has poor high-temperature stability; thus, it is necessary to improve its high-temperature stability. The addition of a high-temperature stabilizer to alumina can improve its high-temperature stability. A study has shown that the high specific surface area of activated alumina can be maintained by doping La to inhibit the crystal transformation of Al_2O_3 at 1,200°C (Wei et al., 2005). In addition, studies have revealed that a strong two-phase symbiosis can be formed between CeO_2 and Al_2O_3 in the process of synthesizing CeO_2-Al_2O_3, thus making CeO_2 and Al_2O_3 to be evenly distributed in the symbiotic process, hindering the agglomeration and crystal transformation of oxides, and improving the stability of γ-Al_2O_3 under high-temperature conditions (Li et al., 2010). The above studies showed that the doping of rare Earth and alkaline Earth metal could improve the high-temperature stability of active Al_2O_3. The active Al_2O_3 carriers doped with alkaline Earth and rare Earth metals (La, Ce, and Ba) were synthesized *via* a sol-gel method to explore the influence of various element dopings on the active Al_2O_3 prepared *via* a sol-gel method. The influence of rare Earth and alkaline Earth metal doping on the high-temperature stability of active Al_2O_3 and its mechanism was studied using Brunauer–Emmett–Teller (BET), X-ray diffraction, Fourier-transform infrared spectroscopy, Scanning electron microscopy, and transmission electron microscopy.

2 Materials and methods

2.1 Materials

The materials used in the experiment were as follows: aluminum nitrate (AR), ethanol (AR), propylene oxide (AR), ammonia (concentration of 15%–28%), lanthanum nitrate (AR), cerium nitrate (AR) and barium hydroxide (AR). All chemicals were purchased from the Chengdu KeLong Chemical Reagent Plant. The deionized water used in this study was produced in the laboratory. The formula for synthesizing activated alumina is shown in Table 1. The dosages of lanthanum nitrate, cerium nitrate, and barium hydroxide used in the experiment are presented in Tables 2–Tables 4, respectively.

TABLE 4 Experimental formula of different addition amounts of barium hydroxide.

Number	Dosage (mole percentage of aluminum nitrate)
Ba-1%	1
Ba-2%	2
Ba-4%	4
Ba-8%	8
Ba-16%	16

2.2 Preparation of modified Al_2O_3

Aluminum nitrate, lanthanum nitrate, cerium nitrate, and barium hydroxide were added to the mixed solution of ethanol and water. For the mixed doping sample, the two-phase mixture was prepared according to the two-phase ratio of 1:1 and the total addition was 1%, and the three-phase mixture sample was doped according to the three-phase ratio of 1:1:1 and the total addition was 1%. The mixed solution was continuously stirred until all particles were completely dissolved in the solution. Propylene oxide was slowly added to the beaker containing the mixed solution. Then, the mixed solution was stirred at high speed for 5–6 min to ensure propylene oxide was evenly distributed in the solution. Afterward, ammonia water was slowly dropped into the beaker and stirred for 10–11 min until the solution became colorless and transparent. Then the mixed solution in the beaker was allowed to stand at room temperature, aging for 24 h, to form a wet gel. The obtained wet gel was placed into an oven and dried

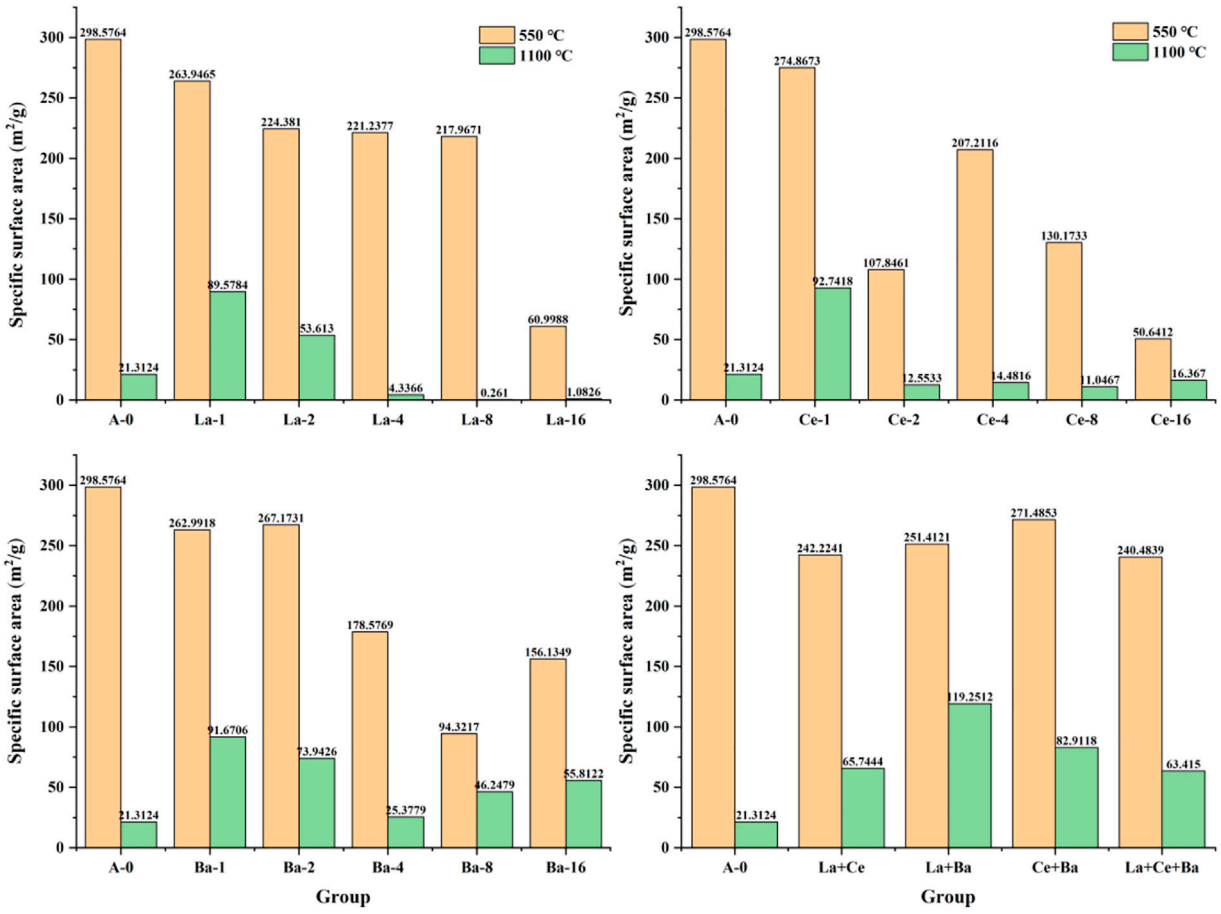

FIGURE 1
Specific surface area of pure activated alumina, single doping modified alumina and mixed doping-modified alumina.

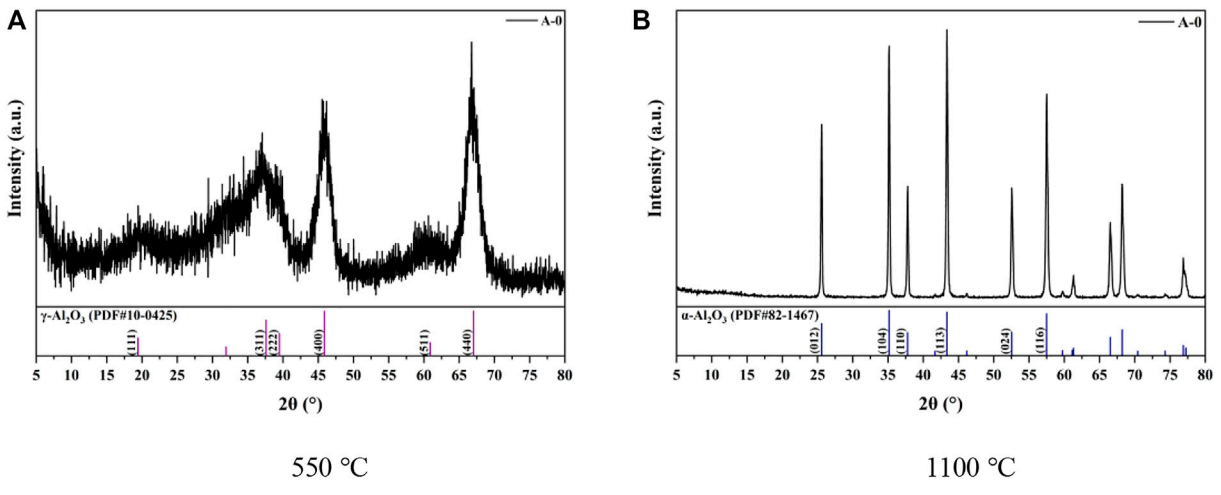

FIGURE 2
XRD pattern of Al_2O_3 calcined at 550°C and aged at 1,100°C.

at 60°C for 24 h. Afterward, the dried gel was transferred into a resistance furnace and calcined at 550°C for 4 h at a heating rate of 5°C/min. Then, the calcined product was cooled to obtain modified Al_2O_3. Then, the heat treatment aging test was performed at 1,100°C for 4 h, and the changes in specific surface area and phase were investigated.

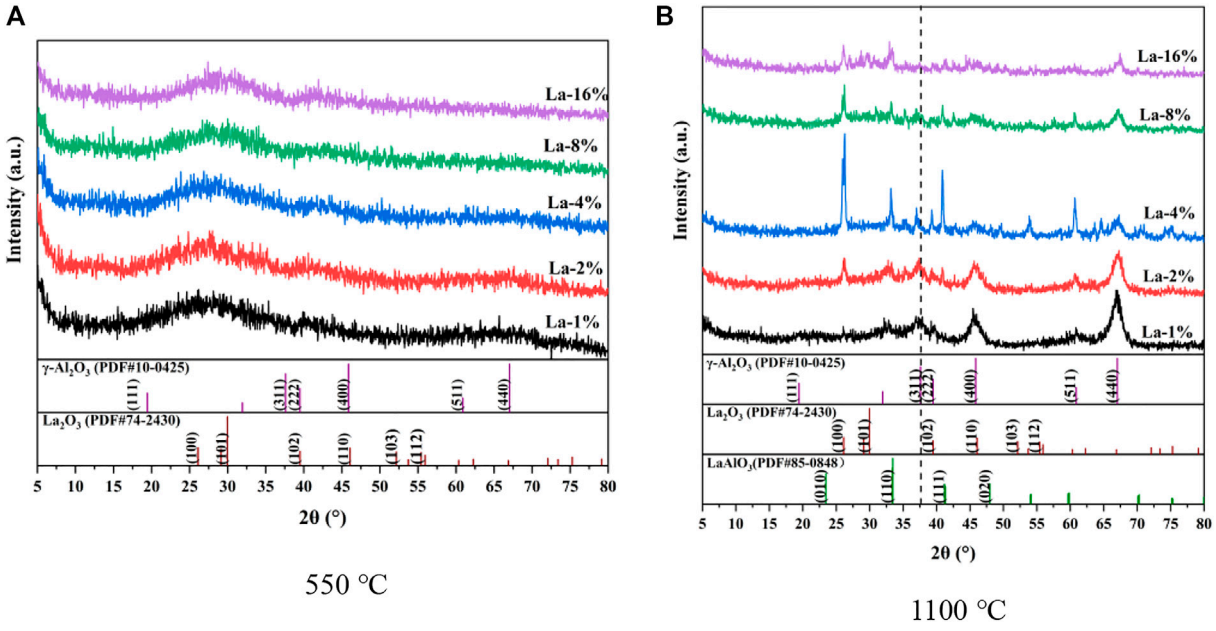

FIGURE 3
XRD pattern of La-doped sample calcined at 550°C and aged at 1,100°C.

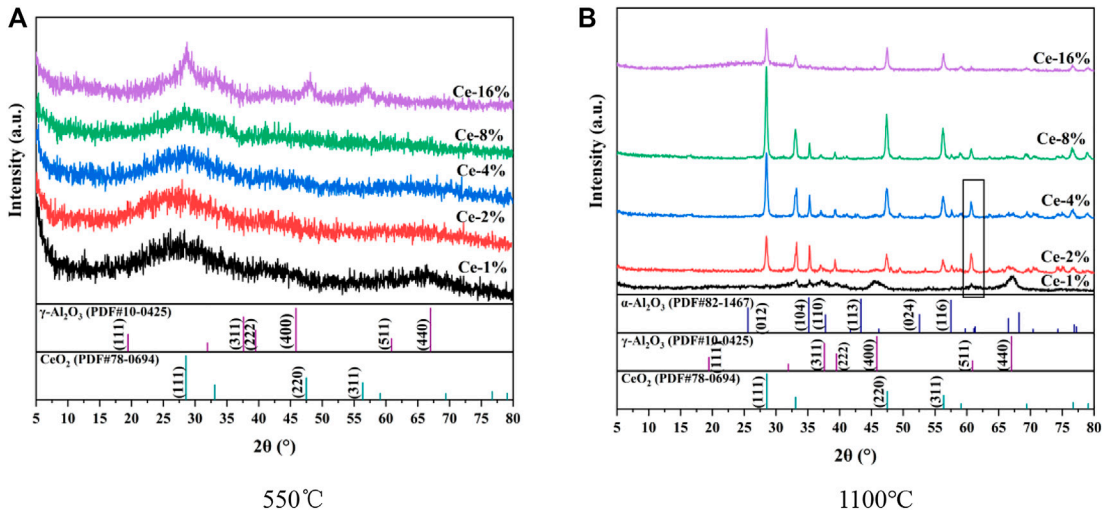

FIGURE 4
XRD pattern of Ce-doped sample calcined at 550°C and aged at 1,100°C.

2.3 Characterization of samples

The X-ray diffractometer (XRD, DX-2700B) was used to test the diffraction pattern of the synthesized activated alumina. The scanning step was 0.04°, and the scanning angle 2θ ranged from 5° to 80°.

The specific surface area of the synthesized activated alumina was measured by a fully automatic physical adsorption instrument (BET, Micromeritics ASAP2460). Before the measurement, the sample was dried at 300°C for 4 h to remove the water and air in the sample, and then the nitrogen adsorption experiment was performed at 77 K. BET was used to calculate the specific surface area.

The molecular structure and chemical bonds of the synthesized activated alumina were analyzed using a Fourier transform infrared spectrometer (FT-IR, NICOLET 6700). The sample was mixed with potassium bromide at a mass ratio of 1:100 and ground evenly in an agate mortar. The samples obtained after mixing were pressed into thin sheets and tested in the range of 4,000–400 cm^{-1}.

The microstructure and pore distribution of the synthesized alumina were examined using a scanning electron microscope (SEM, ZEISS EV0 MA15) and transmission electron microscope (TEM, ZEISS Libra 200 FE). A small amount of ground sample was added to anhydrous ethanol and ultrasonically dispersed for

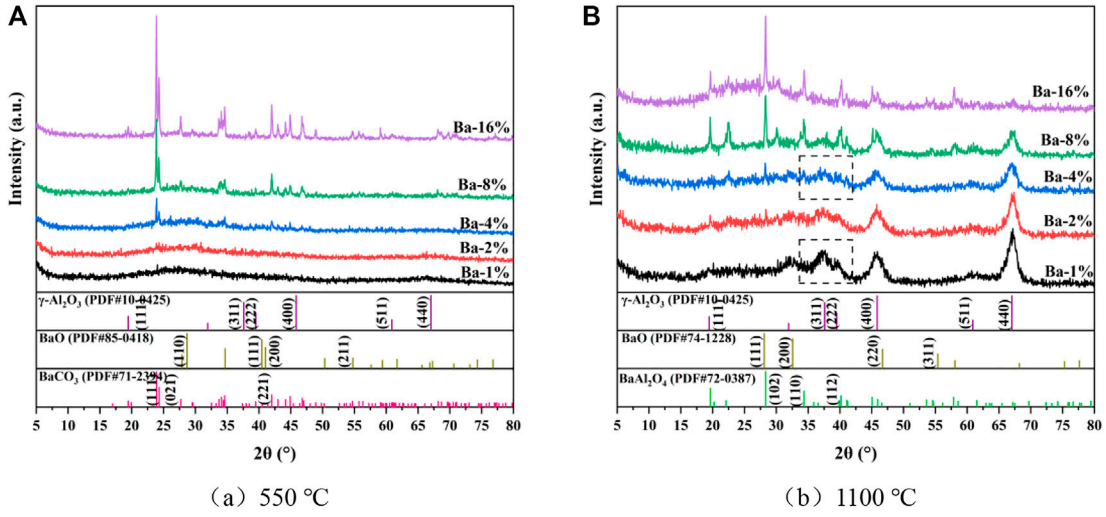

（a）550 ℃　　（b）1100 ℃

FIGURE 5
XRD pattern of Ba-doped sample calcined at 550°C and aged at 1,100°C.

30 min. Then one drop of ethanol mixed solution was gently dropped onto a clean glass sheet using a dropper. After the ethanol was volatilized, the sample on the glass plate was collected with conductive adhesive and sprayed with gold. Afterward, the sprayed sample was examined using SEM. In addition, one drop of ethanol was added to the mixture onto the copper gate, and the sample was examined using TEM after ethanol volatilization.

3 Results and discussion

3.1 Specific surface area analysis

Considering the special application performance as catalyst support, the specific surface area of Al_2O_3 prepared under different conditions was tested. Figure 1 shows the specific surface area of pure activated alumina and samples doped with La, Ce, and Ba calcined at 550°C and aged at 1,100°C for 4 h. The specific surface areas of pure synthesized Al_2O_3 obtained after its calcination and high-temperature aging at 550°C and 1,100°C were 298.5764 and 21.3124 m^2/g, respectively, indicating that the specific surface area of Al_2O_3 after high-temperature aging was significantly reduced. The specific surface area of all modified samples was smaller than that of pure Al_2O_3 after calcination at 550°C. When the high-temperature stabilizers La, Ce, and Ba were added to the sample, the specific surface area of the sample showed a downward trend with increasing content. After the sample with 1% of La, Ce, and Ba contents was aged at a high temperature of 1,100°C, the specific surface area became the largest. When the contents of La, Ce, and Ba were more than 1%, the specific surface area of the sample decreased in a "cliff-like" manner, and the specific surface area of the sample doped with La significantly decreased. It is worth noting that when the specific surface area of Ce-2 and Ba-8 changes significantly, this is because the addition of Ce-2 and Ba-8 has a significant effect on the size of primary Al_2O_3 crystallization particles, thus affecting the pore structure. Overall, the modification effect of Ba was the best, and the specific surface area of all the samples was higher than that of pure Al_2O_3 after they were aged at a high temperature of 1,100°C.The specific surface area of "La + Ba" mixed sample after high-temperature aging at 1,100°C for 4 h was the largest (119.2512 m^2/g). The high-temperature stability of other mixed-doped samples has not been further improved. The specific surface area of the other groups after high-temperature aging at 1,100°C was lower than that of the samples when each component was doped separately, indicating that there was an interaction between the doped elements.

3.2 Phase analysis

Figure 2 shows the XRD pattern of pure Al_2O_3 calcined at 550°C (Figure 2A) and aged at 1,100°C for 4 h (Figure 2B). After the pure Al_2O_3 was calcined at 550°C, only the diffraction characteristic peak of γ-Al_2O_3 (PDF # 10-0425) was observed in the spectrum. After the sample was aged at a high temperature of 1,100°C, only the diffraction characteristic peak of α-Al_2O_3 (PDF # 82-1467) was observed in the spectrum, indicating that γ-Al_2O_3 transformed into α-Al_2O_3 after high-temperature treatment at 1,100°C, thus decreasing the specific surface area of pure Al_2O_3.

Figure 3 shows the XRD pattern of La-doped samples calcined at 550°C (Figure 3A) and aged at 1,100°C for 4 h (Figure 3B). As shown in Figure 3A, only diffraction characteristic peaks of γ-Al_2O_3 (PDF#10-0425) and La_2O_3 (PDF#74-2430) were observed in the spectrum after the calcination of the samples at 550°C. No significant decrease was observed in the diffraction peaks of La_2O_3 as La content increased. This phenomenon can be attributed to low calcination temperature and crystallization degree of La_2O_3. As shown in Figure 3B, γ-Al_2O_3 (PDF#10-0425) (Chen et al., 2018), La_2O_3 (PDF#74-2430), and $LaAlO_3$ (PDF#74-2430) were observed in the sample after it was aged at 1,100°C. The diffraction characteristic peak at 1,100°C was sharper, indicating that high temperature could promote the formation and growth of crystals.

When the content of La was less than 4%, the intensity of the characteristic peak of γ-Al_2O_3 gradually weakened, and the diffraction characteristic peak corresponding to the (311) crystal plane shifted to

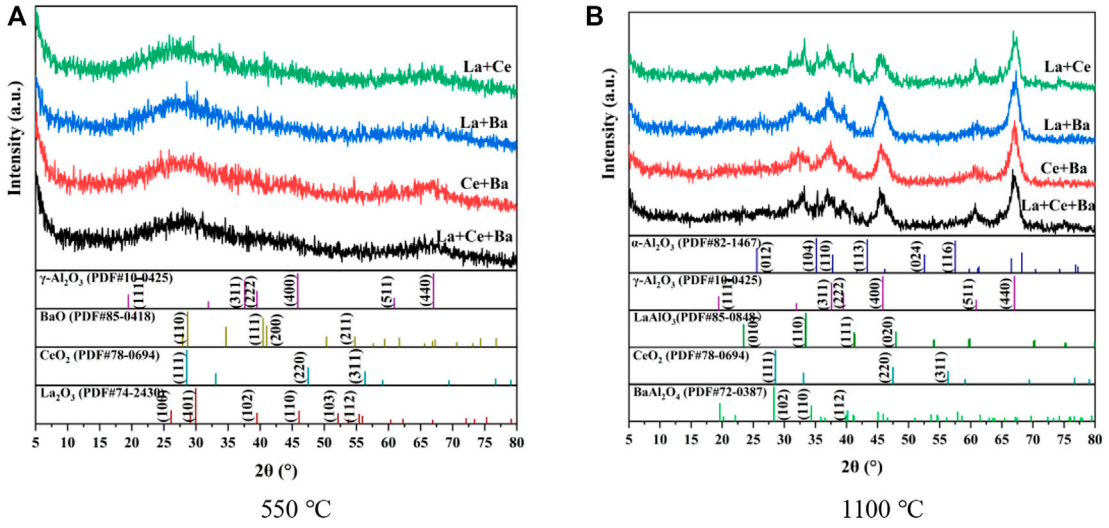

FIGURE 6
XRD pattern of mixed doping after calcination at 550°C and aged at 1,100°C.

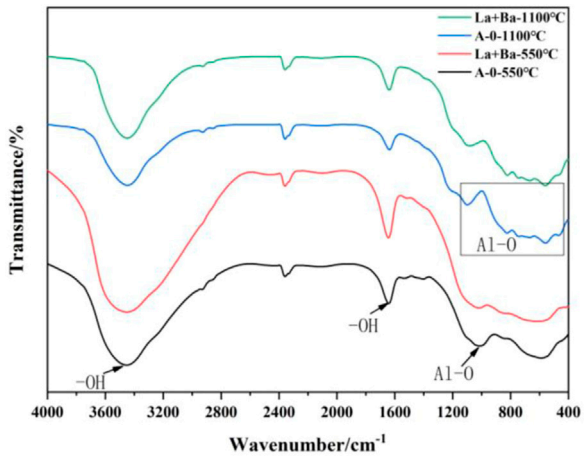

FIGURE 7
Infrared spectra of modified Al_2O_3 before and after aging.

the left because the introduction of La element led to the distortion of the Al_2O_3 lattice (Gong et al., 2001). With the increased La content, La reacted with activated alumina to form $LaAlO_3$ (Jing et al., 2020); thus, the corresponding characteristic peak intensity gradually increased. When the content of La was more than 4%, the characteristic peak of $LaAlO_3$ gradually increased, and the BET test results showed that the corresponding specific surface area was less than 2 m^2/g, which was due to the thermally stable product of La atoms covering the surface of Al_2O_3 (BETTMAN et al., 1989).

Figure 4 shows the XRD patterns of Ce-doped samples after calcination at 550°C (Figure 4A) and aging at 1,100°C for 4 h (b). After the calcination of Ce-doped samples at 550°C, the characteristic peaks of γ-Al_2O_3 (PDF#10-0425) and CeO_2 (PDF#78-0694) are presented in Figure 4A. The result showed that the diffraction characteristic peak of CeO_2 was significantly enhanced with increasing Ce content. When the Ce content was 16%, a clear diffraction characteristic peak appeared, indicating that the crystallization degree of CeO_2 in alumina increased; Figure 4B shows the characteristic peak of α-Al_2O_3 (PDF82-1467) after aging the samples at 1,100°C.

The addition of Ce inhibited the transformation of γ-Al_2O_3 to α-Al_2O_3. The crystallization degree of CeO_2 was related to the content of CeO_2. The crystallization degree of CeO_2 increased when the content of CeO_2 was below 8%. By comparing the samples with Ce content of 1, 2, and 4%, the diffraction characteristic peaks corresponding to (511) of γ-Al_2O_3 containing Ce content of 2% and 4% increased significantly, indicating that Ce element had the effect of inducing Al_2O_3 lattice distortion. Compared with the spectrum at 550°C, the crystallinity of CeO_2 crystal was higher with the increase in temperature under the same dosage condition, indicating that high temperature contributed to the formation of CeO_2. The above results show that Ce atoms mainly exist in the form of CeO_2, and the presence of Al_2O_3 does not interfere with the formation of CeO_2 (Lu et al., 2003; Pang et al., 2020).

Figure 5 shows the XRD pattern of Ba-doped samples aged at 550°C (Figure 5A) and 1,100°C (Figure 5B) for 4 h. After calcination of Ba-doped samples at 550°C, the characteristic peaks of γ-Al_2O_3 (PDF#10-0425), BaO (PDF#74-1228), and $BaCO_3$ (PDF#71-2394) are shown in Figure 5A. After the aging of Ba-doped samples at 1,100°C, the characteristic peaks of γ-Al_2O_3 (PDF#10-0425), BaO (PDF#74-1228), and $BaAl_2O_4$ (PDF#72-0387) are shown in Figure 5B. The result showed $BaCO_3$ decomposed after it was aged at 1,100°C. When the Ba content was less than 4%, the characteristic peak intensity of γ-Al_2O_3 gradually decreased with the increasing Ba content. A weak characteristic peak of $BaAl_2O_4$ was observed at 4% addition of Ba, which indicated that Ba^{2+} existed in the lattice gap of alumina after the decomposition of $BaCO_3$ (Chen et al., 2021), resulting in the distortion of alumina lattice and the interaction with alumina to form $BaAl_2O_4$ (Jing et al., 2021). At the same time, compared with the XRD patterns of samples with 1% and 4% Ba content, the characteristic peaks corresponding to γ-Al_2O_3 (311)

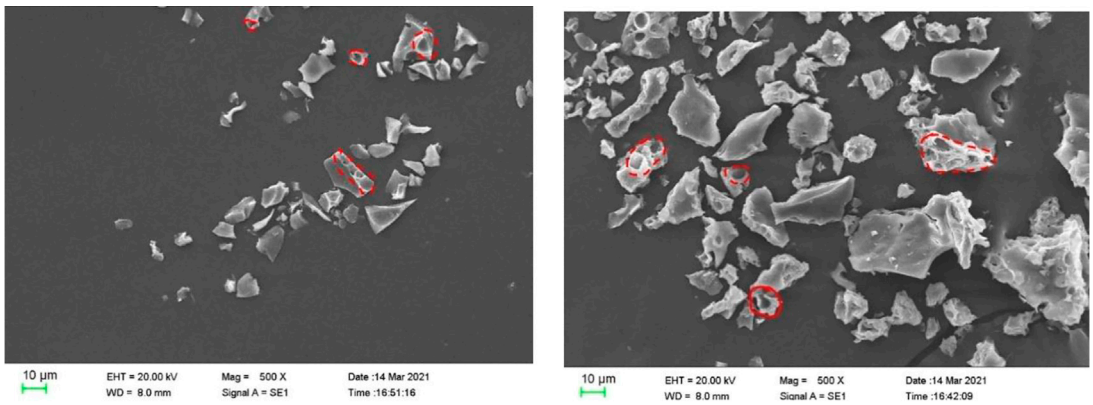

FIGURE 8
SEM image after aging at 1,100°C.

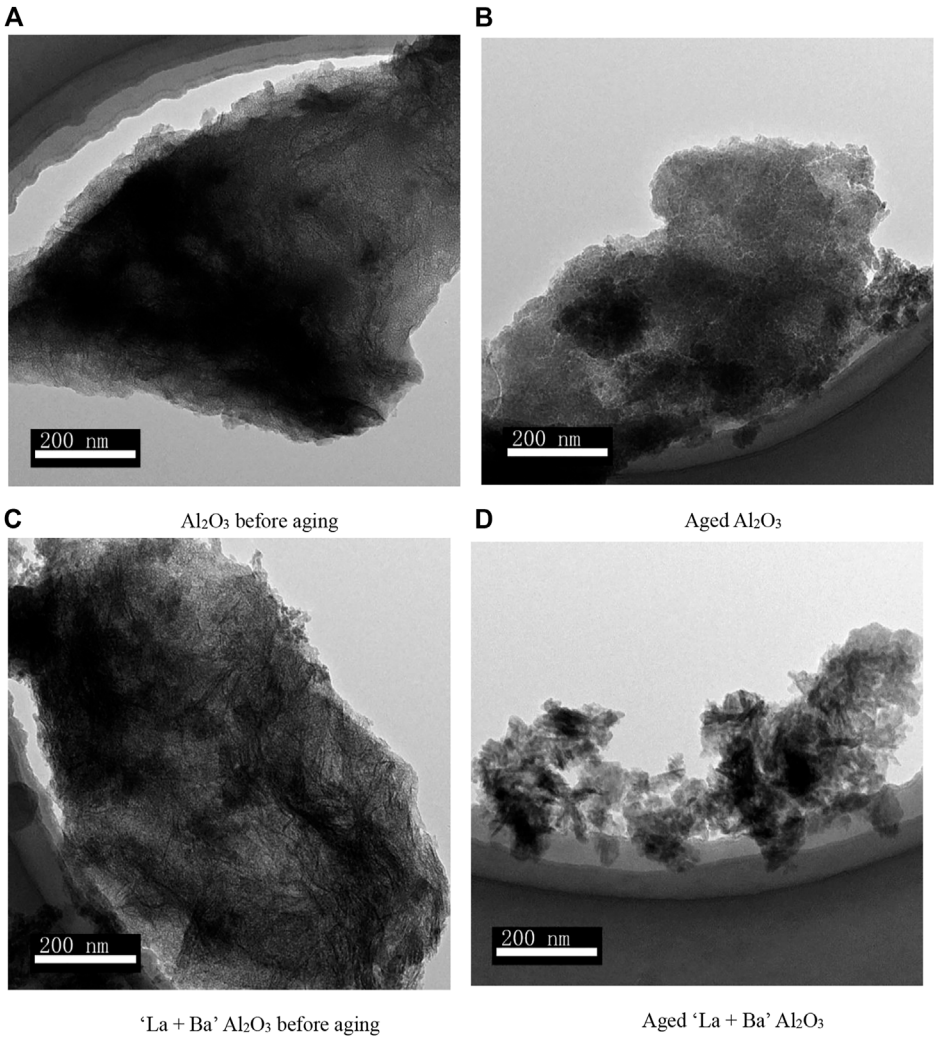

FIGURE 9
TEM images before and after aging at 1,100°C.

and (222) rapidly disappeared. When the Ba content was 4%, the corresponding characteristic peaks disappeared, but (440) and (400) still exhibited sharp diffraction characteristic peaks, which further indicated that the introduction of Ba atoms led to the distortion of alumina crystals. When the Ba content was more than 4%, the characteristic peak of $BaAl_2O_4$ appeared in the sample, and the characteristic peak of α-Al_2O_3 (PDF#82-1467) was not observed. The $BaAl_2O_4$ and α-Al_2O_3 were both hexagonal close-packed structures. Only the characteristic peak of $BaAl_2O_4$ appeared after the sample was calcined at a high temperature, indicating that the crystal structure of the former was more stable. The addition of Ba inhibited the transformation of γ-Al_2O_3 to α-Al_2O_3. The specific surface area of the sample with 16% of Ba content was much higher than that of La and Ce samples with the same content owing to a large specific surface area of $BaAl_2O_4$ (Yang et al., 2015; Yadav and Sharma, 2019).

Figure 6 shows the XRD pattern of the samples calcined at 550°C (Figure 6A) and aged at 1,100°C for 4 h (Figure 6B), with the sample containing 1% content of La, Ce, and Ba. The characteristic peaks of γ-Al_2O_3 (PDF#10-0425), La_2O_3 (PDF#74-2430), and CeO_2 (PDF#78-0694) after calcination at 550°C are shown in Figure 6A. Most of the aluminas retained their amorphous structures after calcination. After the samples were aged at 1,100°C, the characteristic peaks of α-Al_2O_3 (PDF#82-1467), γ-Al_2O_3 (PDF#10-0425), $LaAlO_3$ (PDF#85-0848), CeO_2 (PDF#78-0694), and $BaAl_2O_4$ (PDF#72-0387) are shown in Figure 6B. After La and Ce were co-doped, the characteristic peak of $LaAlO_3$ containing 1% content of La was observed, and the characteristic peak of CeO_2 was significantly enhanced, indicating the existence of an interaction between La and Ce (Tang et al., 2018), which could promote the formation of $LaAlO_3$ and CeO_2. After the incorporation of Ba and Ce, α-Al_2O_3 diffraction peaks appeared, indicating that the inhibition of Ba and Ce on the phase transition of Al_2O_3 is interfered with each other, which may be related to the electron arrangement of the them. After La and Ba were doped, the diffraction characteristic peaks of $BaAl_2O_4$ were observed in the spectrum, and the diffraction characteristic peaks of (311) and (222) corresponding to γ-Al_2O_3 were more visible than those of single doping of Ba. This phenomenon indicated that the introduction of Ba atoms distorted the alumina crystal, and the doped La atoms could induce the distortion and promote the formation of $BaAl_2O_4$. The XRD patterns of "La + Ce" doped with three elements were similar to that of "La + Ce" doped. However, the diffraction characteristic peak of α-Al_2O_3 was more visible; as a result, the specific surface area of this group was the lowest, indicating mutual interference between the elements when the three elements were doped, which reduced the inhibitory effect of the crystal transformation of alumina.

3.3 Infrared spectroscopic analysis

Based on the above discussion results, this section discusses the functional group changes on the surface of Al_2O_3 before and after doping and modification with La + Ba As shown in Figure 7, the corresponding infrared spectra of each sample are mainly the vibration peaks of -OH and Al-O (Xu et al., 2022). Among them, the stretching vibration at 3,450 and 1,644 cm^{-1} corresponds to that of -OH, and the vibration at 1,030 cm^{-1} corresponds to that of Al-O. Studies have shown that the essence of the sintering phase transition process of Al_2O_3 is its dehydroxylation process (Wu et al., 2021). For the sample treated at 550°C, the peak area of La + Ba doped modified Al_2O_3 sample is larger at 3,450 cm^{-1}, and the strength value is higher. This means that the modified sample has a higher content of γ-Al_2O_3. In the sample treated at 1,100°C, the diffraction peak area at 3,450 cm^{-1} is smaller, which indicates that the transition from γ-Al_2O_3 to α-Al_2O_3 is irreversible.

Compared with the spectra of modified samples containing La + Ba after aging at 1,100°C, the peak areas of undoped samples at 3,450 and 1,644 cm^{-1} were smaller, indicating that the modified samples retained more -OH, that is, more γ-Al_2O_3. The results of the infrared analysis showed that the incorporation of La + Ba could hinder the crystal transformation of alumina, which was consistent with the XRD test results. Numerous Al-O vibration peaks at 1,101, 826, 665, 558, and 462 cm^{-1} were observed in the fingerprint region (Hiremath et al., 2020), indicating the formation of the Al-O-Al bond and the corresponding oxygen ion vacancies in the structure (Feng et al., 2011; Belekar and Dhoble, 2018; Li et al., 2020; Yang et al., 2020). La and Ba atoms affected the diffusion and rearrangement of $O^{2-}$and Al^{3+} by occupying the corresponding lattice vacancies (Arai and Machida, 1996; Ozawa and Nishio, 2016).

3.4 Morphological observation

Figure 8 shows the SEM image of the sample after aging at 1,100°C for 4 h. The samples before and after aging were tested using TEM to better compare the microstructure difference before and after aging. Figure 9 shows the TEM image of the sample before and after aging. Under the condition of 500 times magnification, the pure Al_2O_3 synthesized using the sol-gel method had an irregular polyhedron shape, and the surface was mainly flat and smooth, with only a few depression marks, and the diameter was about 3–8 μm (Figure 8). The Al_2O_3 modified by doping had a rough surface, with clear gaps and folds, and more holes. The size of the holes was larger than that of the pure Al_2O_3. As shown in Figure 8, the TEM image of pure Al_2O_3 before aging was fog-like. The interior of the pure Al_2O_3 mainly contained fine particles, and each particle was evenly distributed, with abundant pores between the particles. TEM images revealed cracks in the samples after aging, and there were agglomerations between the particles, indicating that the pores of Al_2O_3 were reduced during the transformation from γ phase to α phase after high-temperature aging, thus significantly decreasing specific surface area. The observed cracks were attributed to different orientations between grains. The La and Ba-modified samples displayed thick dark lines in the TEM images before aging, and other samples were similar to the TEM images of pure Al_2O_3 before aging. By comparing the TEM images after aging, the pores in the samples doped with La and Ba were reduced. However, the agglomerated products of the modified samples were significantly larger than those of pure Al_2O_3 samples after calcination, indicating that the transition from γ phase to α phase was insignificant.

4 Conclusion

In this study, active Al_2O_3 was synthesized *via* a sol-gel method. La, Ce, and Ba were used as high-temperature stabilizing additives. The effects and mechanism of different contents of La, Ce, Ba, and mixed doping on active Al_2O_3 were investigated.

1) La, Ce, and Ba inhibited the crystal transformation from γ-Al_2O_3 to α-Al_2O_3, and the incorporation of 1% Ba exhibited an excellent inhibitory effect on the crystal transformation. The addition of La and Ba atoms to Al_2O_3 distorted the Al_2O_3 crystal. The crystal structure of $BaAl_2O_4$ was more stable than that of α-Al_2O_3. The O atoms in Al_2O_3 preferentially combined with Ce atoms to form CeO_2.
2) The co-doping of La and Ba exhibited the best inhibitory effect on the crystal transformation of active Al_2O_3. XRD analysis results revealed a synergistic effect between La and Ce, which promoted the formation of $LaAlO_3$ and CeO_2. Ba atoms caused the distortion of alumina crystal, while the doped La atoms accelerated the distortion and promoted the formation of $BaAl_2O_4$. The infrared analysis results showed that the modified sample retained more γ-Al_2O_3. SEM analysis revealed the rough surface of active Al_2O_3 and gaps on the surface after the mixed modification of the sample with La and Ba. TEM analysis results showed that La and Ba inhibited the crystal transformation of active Al_2O_3.

Data availability statement

The raw data supporting the conclusion of this article will be made available by the authors, without undue reservation.

Author contributions

ZW: Conceptualization, investigation, writing-original draft, data curation. LJ: Validation, resources, writing—review and editing, supervision. QD: Validation, formal analysis, investigation, data curation. QG: Formal analysis, project administration. JC: Formal analysis, project administration. XC: Methodology, conceptualization.

Funding

The authors appreciate the support of the Sichuan Science and Technology Program (2021YFQ0045 and 2021YFSY0056) and the Cnooc's preliminary project: Feasibility study of Wenchang 9-7 oilfield (2021PFS-05). This study was financially supported by 111 Project, No. D18016.

Acknowledgments

The authors would also like to thank the Advanced Cementing Materials Research Center of SWPU for their kind assistance with the experiments.

Conflict of interest

Authors ZW and LJ were employed by the company CNOOC Research Institute Co., Ltd. and author QD was employed by the company Exploration Business Department of PetroChina Southwest Oil and Gas Field Company.

The remaining authors declare that the research was conducted in the absence of any commercial or financial relationships that could be construed as a potential conflict of interest.

Publisher's note

All claims expressed in this article are solely those of the authors and do not necessarily represent those of their affiliated organizations, or those of the publisher, the editors and the reviewers. Any product that may be evaluated in this article, or claim that may be made by its manufacturer, is not guaranteed or endorsed by the publisher.

References

Aghamohammadi, S., Haghighi, M., Maleki, M., and Rahemi, N. (2017). Sequential impregnation vs. sol-gel synthesized Ni/Al_2O_3 -CeO_2 nanocatalyst for dry reforming of methane: Effect of synthesis method and support promotion. *Molecular Catalysis* 431, 39–48. doi:10.1016/j.mcat.2017.01.012

Arai, H., and Machida, M. (1996). Thermal stabilization of catalyst supports and their application to high-temperature catalytic combustion. *Applied Catalysis A: General* 138, 161–176. doi:10.1016/0926-860x(95)00294-4

Azizi, Y., Kambolis, A., Boréave, A., Giroir-Fendler, A., Retailleau-Mevel, L., Guiot, B., et al. (2016). NO_x abatement in the exhaust of lean-burn natural gas engines over Ag-supported γ-Al_2O_3 catalysts. *Surface Science* 646, 186–193. doi:10.1016/j.susc.2015.10.020

Belekar, R. M., and Dhoble, S. J. (2018). Activated Alumina Granules with nanoscale porosity for water defluoridation. *Nano-Structures Nano-Objects* 16, 322–328. doi:10.1016/j.nanoso.2018.09.007

Bettman, M. C. R. E., Otto, K., et al. (1989). Dispersion studies on the system of La_2O_3/γ-Al_2O_3. *J. Catal.* 117 (2), 447–454. doi:10.1016/0021-9517(89)90354-0

Chen, X., Lin, J., Zheng, Y., Zhan, Y., Zhang, W., Xiao, Y., et al. (2021). Catalytic methane oxidation performance over Pd/γ-Al_2O_3 catalyst optimized by the synergy of phosphorus and MO_x (M = La, Ba and Zr). *Fuel* 299, 120933. doi:10.1016/j.fuel.2021.120933

Chen, X., Zheng, Y., Huang, F., Xiao, Y., Cai, G., Zhang, Y., et al. (2018). Catalytic activity and stability over nanorod-like ordered mesoporous phosphorus-doped alumina supported palladium catalysts for methane combustion. *ACS Catal.* 8 (12), 11016–11028. doi:10.1021/acscatal.8b02420

Deng, S., and Zhou, J. (2020). Research progress of automobile exhaust pollution control technology. *Chemical Design Newsletter* 46 (8), 213–214. in Chinese.

Feng, G., Huo, C., Li, Y., Wang, J., and Jiao, H. (2011). Structures and energies of iron promoted γ-Al2O3 surface: A computational study. *Chemical Physics Letters* 510 (4-6), 224–227. doi:10.1016/j.cplett.2011.05.035

Feng, Z., Ren, Q., Peng, R., Mo, S., Zhang, M., Fu, M., et al. (2019). Effect of CeO_2 morphologies on toluene catalytic combustion. *Catalysis Today* 332, 177–182. doi:10.1016/j.cattod.2018.06.039

Gong, C. M., Lin, Z. E., Gao, S. J., et al. (2001). Study on the preparation chemistry of new high-temperature and high-surface alumina materials Ⅳ. The influence of lanthanum composition on the preparation of high-surface-area Al_2O_3 by sol-gel method. *Journal of Fuel Chemistry and Technology* 1, 76–79. in Chinese.

Hiremath, V., Shiferraw, B. T., and Seo, J. G. (2020). MgO insertion endowed strong basicity in mesoporous alumina framework and improved CO_2 sorption capacity. *Journal of CO_2 Utilization* 42, 101294. doi:10.1016/j.jcou.2020.101294

Hosseini, Z., Taghizadeh, M., and Yaripour, F. (2011). Synthesis of nanocrystalline γ-Al_2O_3 by sol-gel and precipitation methods for methanol dehydration to dimethyl ether. *Journal of Natural Gas Chemistry* 20 (2), 128–134. doi:10.1016/s1003-9953(10)60172-7

Jing, Y., Cai, Z., Liu, C., Toyao, T., Maeno, Z., Asakura, H., et al. (2020). Promotional effect of La in the three-way catalysis of La-loaded Al_2O_3-supported Pd catalysts (Pd/La/Al_2O_3). *ACS Catalysis* 10 (2), 1010–1023. doi:10.1021/acscatal.9b03766

Jing, Y., Wang, G., Ting, K. W., Maeno, Z., Oshima, K., Satokawa, S., et al. (2021). Roles of the basic metals La, Ba, and Sr as additives in Al_2O_3-supported Pd-based three-way catalysts. *Journal of Catalysis* 400, 387–396. doi:10.1016/j.jcat.2021.06.016

Li, B., Li, S., Wang, Y., Zhang, W., and Lin, B. (2010). Intergrowth effects in CeO_2-Y-Al_2O_3 mixed oxides. *Chinese Journal of Catalysis* 31 (5), 528–534. doi:10.1016/s1872-2067(09)60067-x

Li, L., Gan, Y., Lu, Z., XiaohuYuQing, S., Gao, Z., et al. (2020). The effects of Fe, Co and Ni doping in CuAl2O4 spinel surface and bulk: A dft study. *Applied Surface Science* 521, 146478. doi:10.1016/j.apsusc.2020.146478

Lin, C., Yang, Z., Pan, H., Cui, J., Lv, Z., liu, X., et al. (2021). Ce-introduced effects on modification of acidity and Pt electronic states on Pt-Sn/γ-Al_2O_3 catalysts for catalytic reforming. *Applied Catalysis A: General* 617, 118116. doi:10.1016/j.apcata.2021.118116

Lu, W., Long, J., and Tian, H. (2003). Effects of lanthanum and cerium modification on the properties of alumina. *Journal of Catalysis* 24 (8), 574–578. doi:10.3321/j.issn:0253-9837.2003.08.005

Ministry of Environmental Protection of the People's Republic of China (2020). *China mobile source environmental management annual report*. Beijing, China: Ministry of Environmental Protection of the People's Republic of China. in Chinese.

Ozawa, M., and Nishio, Y. (2016). Thermal stability and microstructure of catalytic alumina composite support with lanthanum species. *Applied Surface Science* 380, 288–293. doi:10.1016/j.apsusc.2015.12.246

Pang, Y., Wu, Y., Chen, Y., Luo, F., and Chen, J. (2020). Degradation effect of Ce/Al_2O_3 catalyst on pyrolysis volatility of pine. *Renewable energy* 162, 134–143. doi:10.1016/j.renene.2020.07.125

Tang, M., Liu, K., Roddick, D. M., and Fan, M. (2018). Enhanced lattice oxygen reactivity over Fe_2O_3/Al_2O_3 redox catalyst for chemical-looping dry (CO_2) reforming of CH_4: Synergistic La-Ce effect. *Journal of Catalysis* 368, 38–52. doi:10.1016/j.jcat.2018.09.022

Tu, L. Q., and Ming, J. (2013). Research on purification and treatment technology of automobile exhaust. *Jiangsu Science & Technology Information* 18, 67. in Chinese. doi:10.3969/j.issn.1004-7530.2013.18.034

Wang, B., Wang, G. L., Sun, L. Z., et al. (2017). Summary of performance improvement of activated alumina coating in automobile exhaust gas purifier. *Hebei College of Industry and Technology* 34 (4), 282–286. in Chinese.

Wei, Q., Chen, Z.-X., Wang, Z.-H., Hao, Y. L., Zou, J. X., and Nie, Z. R. (2005). Effect of La, Ce, Y and B addition on thermal stability of unsupported alumina membranes. *Journal of Alloys and Compounds* 387 (1-2), 292–296. doi:10.1016/j.jallcom.2004.06.081

Wu, Q., Yan, J., Jiang, M., Dai, Q., Wu, J., Ha, M. N., et al. (2021). Phosphate-assisted synthesis of ultrathin and thermally stable alumina nanosheets as robust Pd support for catalytic combustion of propane. *Applied Catalysis B: Environmental* 286, 119949. doi:10.1016/j.apcatb.2021.119949

Xu, H., Zhang, C., Cai, J., Wang, J., Liu, K., and Cheng, X. (2022). Synthesis and characterization of activated alumina with high thermal stability by a low-heat solid-phase precursor method. *Microporous Mesoporous Mater* 337, 111921. doi:10.1016/j.micromeso.2022.111921

Yadav, M., and Sharma, Y. C. (2019). Transesterification of used vegetable oil using $BaAl_2O_4$ spinel as heterogeneous base catalyst. *Energy Conversion and Management* 198, 111795. doi:10.1016/j.enconman.2019.111795

Yadav, S., Mittal, A., Sharma, S., Kumari, K., and Kumar, N. (2021). Highly efficient Ag_2O loaded ZnO/Al_2O_3 coupled catalyst and its photocatalytic application. *Inorganic Chemistry Communications* 130, 108738. doi:10.1016/j.inoche.2021.108738

Yang, G., Li, Y., and Men, Y. (2015). Synergistic catalysis effect of Mn-promoted $BaAl_2O_4$ catalysts on catalytic performance for soot combustion. *Catalysis Communications* 69, 202–206. doi:10.1016/j.catcom.2015.06.020

Yang, W., Li, C., Tian, S., Liu, L., and Liao, Q. (2020). Influence of synthesis variables of a sol-gel process on the properties of mesoporous alumina and their fluoride adsorption. *Materials Chemistry and Physics* 242, 122499. doi:10.1016/j.matchemphys.2019.122499